Title: Hierarchical MTW zeolites in tetrahydropyranylation of alcohols: Comparison of bottom-up and top-down methods

Authors: Ondřej Veselý, Hao Pang, Simon M. Vornholt, Michal Mazur, Jihong Yu, Maksym Opanasenko, Pavla Eliášová

PII: S0920-5861(18)30345-6
DOI: https://doi.org/10.1016/j.cattod.2018.06.010
Reference: CATTOD 11499

To appear in: *Catalysis Today*

Received date: 28-3-2018
Revised date: 27-4-2018
Accepted date: 5-6-2018

Please cite this article as: Veselý O, Pang H, Vornholt SM, Mazur M, Yu J, Opanasenko M, Eliášová P, Hierarchical MTW zeolites in tetrahydropyranylation of alcohols: Comparison of bottom-up and top-down methods, *Catalysis Today* (2018), https://doi.org/10.1016/j.cattod.2018.06.010

Hierarchical MTW zeolites in tetrahydropyranylation of alcohols: Comparison of bottom-up and top-down methods

Ondřej Veselý[a], Hao Pang[a,b], Simon M. Vornholt[c], Michal Mazur[a,c], Jihong Yu[b], Maksym Opanasenko[a], Pavla Eliášová[a*]

[a]Faculty of Sciences, Charles University, Hlavova 8, 128 43 Prague 2, Czech Republic
[b]State Key Laboratory of Inorganic Synthesis & Preparative Chemistry, Jilin University, Changchun, China
[c]School of Chemistry, EaStChem, University of St. Andrews, North Haugh, St. Andrews, Fife, KY16 9ST, United Kingdom

* Corresponding author. Tel. +420 605 930 556. Email address: pavla.eliasova@natur.cuni.cz

Graphical abstract

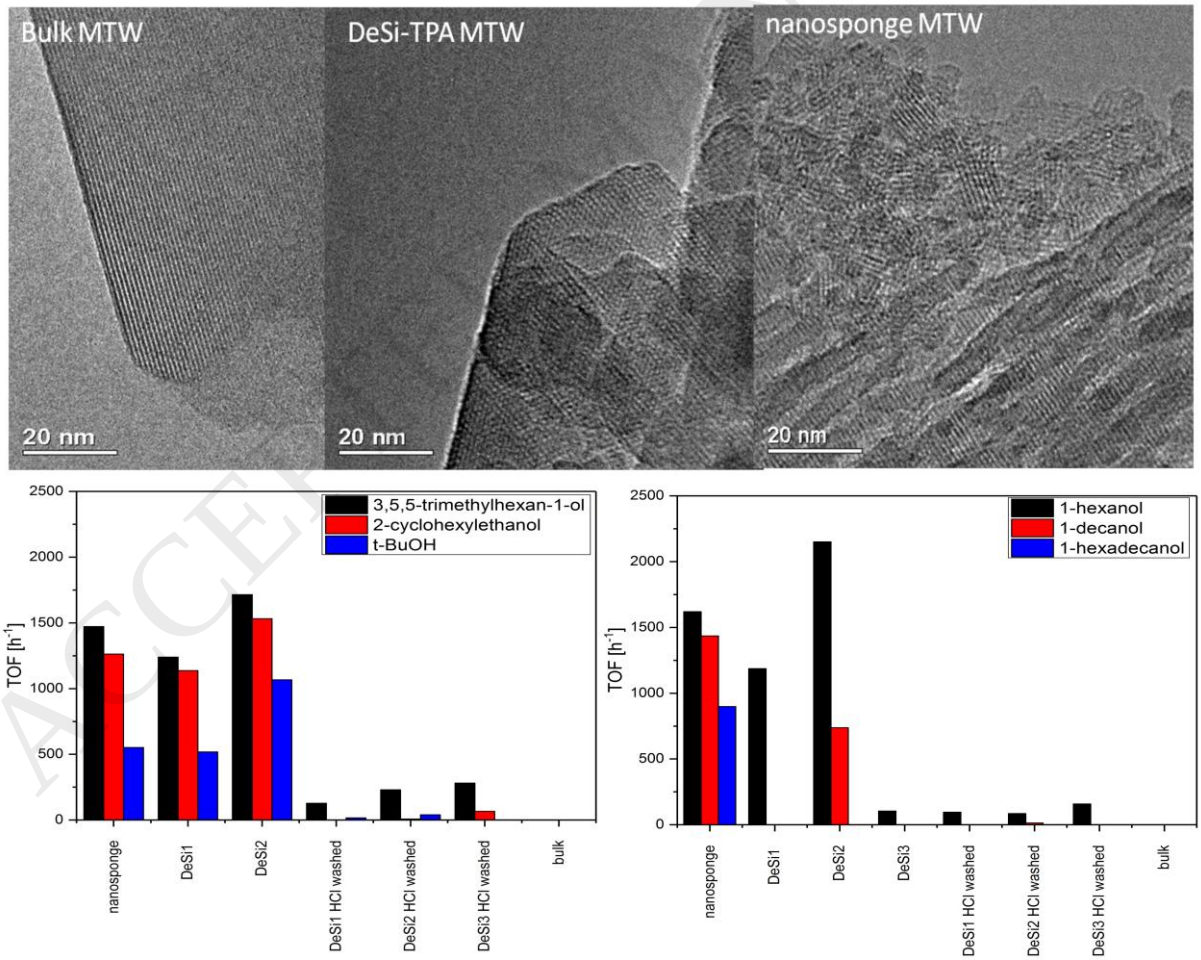

Highlights

- Desilication in presence of tetraalkylammonium ions (TAA^+) caused pore blockage
- Micro- and mesopores can be unblocked by subsequent acid treatment
- High fraction of released pores resulted in the limited mass transfer of reactants
- In tetrahydropyranylation of alcohols the nanosponge exhibited the highest conversions
- In reaction of branched alcohols TAA^+ desil. zeolites excelled based on TOF values

Abstract

Despite a widespread application of zeolites in catalysis, these microporous materials still suffer from a low accessibility of active sites located deep in crystals due to limited size of channels (< 1nm). Here, we prepared a series of micro-mesoporous zeolites with MTW topology and similar Si/Al molar ratio (50). Two topical approaches were applied here: i. bottom-up synthesis with a surfactant-SDA leading to so-called nanosponge material; ii. top-down desilication of bulk crystals by NaOH solution in the presence of tetraalkylammonium cations (TAA^+). Prepared materials were characterized by powder X-ray diffraction, sorption of nitrogen, adsorption of pyridine and di-tert-butyl-pyridine followed by FTIR, solid state ^{27}Al NMR, ICP-OES, SEM, TEM, and STEM-EDS. It was found that the desilication of MTW in the presence of TAA^+ proceeds in different pathway compared to well-studied MFI. This variance was attributed to the different dimensionality of their channel systems (1D vs. 3D). Materials were tested in tetrahydropyranylation of alcohols differing in a chain length and degree of branching. The nanosponge MTW shows generally very good performance. Nevertheless, in cases of the branched alcohols MTW materials desilicated in the presence of TAA^+ exhibited comparable or even higher activity than nanosponge based on TOF values. Therefore, desilicated MTW presents cheaper and equally or more effective catalyst compared to nanosponge material with the same topology.

Keywords: Zeolite; MTW; hierarchical porosity; tetrahydropyranylation of alcohols; nanosponge; desilication

1. Introduction

Zeolites have found a wide range of applications in different fields of chemistry, but most notably as heterogenous catalysts in the oil refining and petrochemical industry. One of their main advantages is so called shape-selectivity provided by their microporous structure, due to which the size and shape of product molecules can be controlled [1-4]. Still, the micropore size ranging usually from 0.25 to 1 nm also presents a major problem, as in the confined space of the micropores diffusion of reactant molecules is severely limited [5]. Ergo, large portion of acid sites located deeper in bulk crystals are left unused. Another consequence is that the size of the micropores makes bulk zeolites unsuitable for transformations of large molecules.

Many different strategies have been studied in order to increase the accessibility of the catalyst´s active sites including synthesis of zeolites in a form of nanocrystals, synthesis of two-dimensional zeolites [6-8] or introducing auxiliary mesoporosity into the material. Probably the most common method is the desilication, which is a selective removal of silicon from the zeolite crystals in a basic solution [9-11]. The advantages of this method are mainly the simplicity and low cost. Although the rate of desilication

can be controlled by multiple factors such as hydroxide solution concentration, duration of the procedure and temperature used, there is no direct control over the size and shape of the created mesopores [12-15]. This may lead to issues with reproducibility of the results. Pérez-Ramírez et al. came up with a novel procedure using so called pore directing agents (PDAs) for the desilication of high-silica ZSM-5 zeolite (MFI topology) [16]. PDA molecules, usually tetraalkylammonium cations (TAA^+), help protecting the zeolite crystals from complete dissolving by adsorption onto their external surface [17]. They create a protective layer and thus, in some extent, allow to narrow down the size of the created mesopores and preserve the microporous structure of the zeolite [16, 18].

Recently, the research has been directed towards synthesizing new advanced hierarchical zeolites with large external surface areas and volumes of mesopores using different approaches [19-23]. These new materials show very promising results in catalysis, nonetheless, their synthesis usually needs special mesopore-templates, e.g. carbon black pearls, carbon nanotubes or specially designed surfactant molecules playing a role of structure-directing-agent (SDA) and PDA at the same time. The last mentioned, surfactant-SDAs, are not commercially available and thus have to be prepared beforehand [23, 24]. Both, the multistep synthesis of surfactant-SDA and the cost of precursor chemicals themselves, dramatically increase the price of the final catalyst and make their real application uncertain from the economical point of view. Therefore, it is worth seeking a cheaper alternative to these materials with comparable catalytic activity. The already well-studied and wide used desilication is a reasonable option. In this research we have focused on desilication with basic solutions in the presence of tetraalkylammonium cations. This approach has been well investigated on one of the most commercially applied zeolite, MFI [16, 18]. Unfortunately, the data for other zeolite topologies desilicated in the presence of TAA^+ are scarce [25, 26]. Hence, our goal is to examine the influence of desilication with TAA^+ solutions on the MTW topology. MTW zeolite can be prepared in a broad range of Si/Al molar ratio (15 - ∞) and its acid sites exhibit high acid strength [27, 28]. It shows excellent catalytic activity and stability with time-on-stream in the cracking of hydrocarbons and in other petroleum refining processes [29-33]. With the one-dimensional 12-ring channel system MTW provides selectivities fitting between medium-pore size MFI (10-10-10-ring channels) and large-pore BEA (12-12-12-ring channels) [34]. Altogether, it makes MTW a potential industrially applicable catalyst [35].

In our work we prepared a set of materials with MTW topology by bottom-up and top-down approaches. Using surfactant-SDA MTW was directly prepared in a hierarchical form called nanosponge. In the top-down approach, bulk MTW crystals were desilicated with three types of basic solutions (tetrapropylammonim hydroxide + NaOH, tetrabutylammoium hydroxide + NaOH and pure NaOH). To examine and compare their catalytic activity we chose tetrahydropyranylation reaction, addition of an alcohol to 3,4-dihydro-2H-pyran forming an ether as a product. The reaction is often used in organic synthesis for protecting hydroxyl groups between individual steps [36]. Advantage of the tetrahydropyranyl group is its good stability in the presence of reducing or alkylating agents as well as some organometallic species such as the Grignard reagents. Moreover, it can be easily unprotected under acidic conditions. Various inorganic acids have been used for the catalysis of the tetrahydropyranylation as well as some heteropolyacids [37, 38]. Nevertheless, many of these acids have lost their popularity due to their negative environmental impact. Zeolites, on the other hand, do occur in nature, cause little or no harm and are no less efficient catalysts for the reaction [39, 40]. Prepared micro-mesoporous MTW materials were tested in the reaction of 3,4-dihydro-2H-pyran with a series of alcohols differing in a chain length and degree of branching.

2. Experimental part

2.1. Synthesis of SDA C22N6

To synthesize the nanosponge MTW zeolite $C_{22}H_{45}–N^+(CH_3)_2–C_6H_{12}–N^+(CH_3)_2–CH_2–(p\text{-}C_6H_4)–CH_2–N^+(CH_3)_2–C_6H_{12}–N^+(CH_3)_2–CH_2–(p\text{-}C_6H_4)–CH_2–N^+(CH_3)_2–C_6H_{12}–N^+(CH_3)_2–C_{22}H_{45}$, further denoted as „C22N6“, was used as a SDA. Its preparation consisted of three steps according to the literature [40]. Firstly, 1-bromodocosane (98 %, TCI) reacted with six times molar excess of *N,N,N',N'*-tetramethyl-1,6-diaminohexane (98 %, TCI). The reactants were mixed in a 1:1 volume mixture of toluene and acetonitrile, using 25 ml of the mixture per 1g of 1-bromodocosane. The reaction was carried out at 60 °C under reflux for 12 hours. The solvents were subsequently evaporated and the product was washed with diethyl ether and dried at room temperature.

The next step was a reaction of the product obtained from the first step with ten times molar excess of 1,4-bis(chloromethyl)benzene (98 %, Sigma-Aldrich) in a 2:1 mixture of chloroform and acetonitrile, using 36 ml of the mixture per 1 g of the precursor. The reaction was carried out at 65 °C under reflux for 24 hours. Afterwards the solvents were evaporated, the product thoroughly washed with diethyl ether and acetone and then dried at room temperature.

The last step was a reaction of *N,N,N',N'*-tetramethyl-1,6-diaminohexane with twice molar amount of the product obtained from the second step in 6.3 ml of chloroform per 1 g of the precursor. The reaction was carried out at 85 °C under reflux for 24 hours. When finished, the chloroform was evaporated, the product was washed with diethyl ether and dried at room temperature.

The purity of each intermediate and final product was checked with ^{1}H NMR spectroscopy.

2.2. Zeolite synthesis

Bulk MTW synthesis

For the synthesis of bulk MTW zeolite tetraethylammonium hydroxide (TEA-OH, 40 % in H_2O, Sigma-Aldrich) was used as SDA. Sodium aluminate (90 %, Riedel-de Haen) was mixed with distilled water and when completely dissolved, TEA-OH was added to the mixture. In a separate vessel colloidal silica (Ludox HS-40, Sigma-Aldrich) was diluted to 30% solution with distilled water. Both solutions were mixed together and stirred until completely homogenous gel. The final molar composition of the gel was 100 SiO_2 : 1 Al_2O_3 : 1.46 Na_2O : 25 SDA : 1330 H_2O. The crystallization was carried out in a Teflon-lined steel autoclave at 160 °C for 6 days under static conditions. The product was separated by filtration, washed with distilled water and dried at 65 °C. The calcination was carried out in a flow of air at 550 °C for 6 hours.

Nanosponge MTW synthesis

Nanosponge MTW zeolite was prepared using the „C22N6“ as SDA as reported in the literature[40]. Sodium aluminate was dissolved in sodium hydroxide (99 %, Lachner) water solution. The mixture was heated up to 60 °C and then the SDA was added and stirred until completely dissolved. The mixture was transferred to a polypropylene bottle, tetraethoxysilane (TEOS, 98 %, Sigma-Aldrich) was added and the whole bottle was shaken intensively to homogenize the gel. Further, an aging was carried out at 60 °C for 20 hours. The crystallization was carried out in a Teflon-lined steel autoclave at 150 °C for 6 days with rotation. The product was filtered, washed with distilled water and dried at 65 °C. The calcination was carried out under a flow of air at 580 °C for 8 hours.

2.3. Desilication of bulk MTW

Desilication of the bulk MTW zeolite was carried out at 65 °C for 30 minutes using three types of solutions: 1) 0.05 M solution of tetrapropylammonium hydroxide (TPA-OH, Acros organics) in 0.2 M solution of sodium hydroxide denoted as „DeSi1“; 2) 0.05 M solution of tetrabutylammonium hydroxide (TBA-OH, Fluka Analytical) in 0.2 M solution of sodium hydroxide, denoted as „DeSi2“; 3) 0.2 M sodium hydroxide solution, denoted as „DeSi3“. Each solution was first heated up to 65 °C and then the bulk MTW zeolite was added in a ratio of 30 ml of the solution per 1 g of the zeolite. After 30 minutes

the vessel was cooled down, zeolite sample filtered off and washed with distilled water until neutral pH. The desilicated sample was dried at 65 °C and calcined in a flow of air at 550 °C for 5 hours. The materials prepared by the first desilication are generally called as the 1st batch.
The same desilication procedure was repeated on the same bulk MTW. Due to the suspicion that after desilication the pores can be blocked by structural debris, each sample was split in half before the calcination. One half of each sample was further stirred in 1M HCl at 60 °C for 4 hours (with ratio 30 ml per 1 g). Subsequently the samples were filtered off, washed with distilled water until neutral pH and dried at 65 °C. All samples, half washed and half unwashed, were calcined in a flow of air at 550 °C for 5 hours. The materials prepared by above procedure are generally named as the 2nd batch.

After preparation of individual samples, each sample was ion-exchanged into NH_4^+-form by stirring with 1M NH_4NO_3 for 4 hours (1 g per 100 ml of solution) and this procedure was repeated four times. Afterwards, the samples were heated at 480 °C for 6 hours (temperature rate 5 °C/ minute) to obtain the samples in H^+-form.

2.4. Characterization

The structure and crystallinity of the zeolites were determined by X-ray powder diffraction using a Bruker AXS D8 Advance diffractometer equipped with a graphite monochromator and a position sensitive detector Våntec-1 using CuKα radiation in Bragg–Brentano geometry.
Nitrogen adsorption/desorption isotherms were measured on a Micromeritics GEMINI II 2370 volumetric Surface Area Analyzer at -196 °C to determine surface area, pore volume and pore size distribution. Before the sorption measurements, all samples were degassed in a Micromeritics FlowPrep 060 instrument under helium at 300 °C (heating rate 10 °C/min) for 4 h. The specific surface area was evaluated by BET method using adsorption data in the range of a relative pressure from p/p0 = 0.05 to p/p0 = 0.25. The t-plot method was applied to determine the volume of micropores (Vmic). The adsorbed amount at relative pressure p/p0= 0.98 reflects the total adsorption capacity (Vtot). The pore size distributions were calculated using the BJH model from the desorption branch of the isotherms.
The concentration and type of acid sites were determined by adsorption of pyridine and di-tert-butylpyridine (DTBPy) as a probe molecule followed by FTIR spectroscopy (Nicolet 6700 AEM module equipped with DTGS detector) using the self-supported wafer technique. Prior to adsorption of the probe molecule, self-supported wafers of zeolite samples were activated in-situ by overnight evacuation at temperature 450 °C. Pyridine adsorption proceeded at 150 °C for 20 min at partial pressure 3 Torr, followed by 20-min evacuation at 150 °C. The concentrations of Brønsted and Lewis acid sites were calculated from integral intensities of individual bands characteristic of pyridine on Brønsted acid sites at 1545 cm^{-1} and band of pyridine on Lewis acid site at 1455 cm^{-1} and molar absorption coefficients of $\varepsilon(B) = 1.67 \pm 0.1$ $cm.\mu mol^{-1}$ and $\varepsilon(L) = 2.22 \pm 0.1$ $cm.\mu mol^{-1}$, respectively [41]. The spectra were recorded with a resolution of 4 cm^{-1} by collection 128 scans for single spectrum. DTBPy adsorption proceeded at 150 °C for 15 min at equilibrium pressure 0.8 Torr, followed by 1 h degassing at the same temperature. The concentration of Brønsted acid sites was calculated from integral intensity of band characteristic of DTBPy on Brønsted acid sites at 1530 cm^{-1} and molar absorption coefficient of $\varepsilon(B) = 1.67 \pm 0.1$ $cm.\mu mol^{-1}$.
Morphology of the samples was studied with scanning electron microscopy using the JEOL JSM-5500LV microscope. Moreover, imaging of the samples was carried out on a FEI Scios Dualbeam SEM, powered by a Schottky FEG electron source and a resolution of 1 nm, equipped with an EDAX Octane Plus EDS, secondary and backscattered electron detector. Operating voltages were 2 kV at 0.1 nA currents at a working distance of 6.7 mm to ensure a sensitive mapping of the particles. The unground samples were placed on an adhesive Leith carbon tab held by an Al-stub disc. To improve conductivity the samples were brushed with Ag-paste and further Au-sputter coated (5 mA per 30 s). EDX analyses were carried as point analyses for 100 seconds.

The high-resolution transmission electron microscopy (HRTEM) was performed using Jeol JEM-2011 electron microscope operating at an accelerating voltage of 200 kV. The HRTEM images were recorded using a 9 Gatan 794 CCD camera. STEM-EDS spectral imaging mapping was performed using FEI Titan™ G2 80–200 STEM with a Cs probe corrector and ChemiSTEM™ technology (X-FEG™ and SuperX™ EDS with four windowless Si drift detectors), operated at 200 kV was used in this study. STEM images were recorded using high-resolution HAADF detector.

Elemental composition of the samples was determined by the ICP-OES method on the Thermo Scientific iCAP 7000. Prior to the measurement samples were mineralized in mixture of concentrated hydrochloric, nitric and hydrofluoric acid.

The solid state ^{27}Al Magic Angle Spinning (MAS) NMR spectra were recorded on an Agilent DD2 500WB spectrometer at resonance frequencies of 130.24. All MAS NMR were carried out with a commercial 3.2 mm triple resonance MAS probe. The chemical shifts of ^{27}Al are referenced to a 1.1 mol/kg solution of $Al(NO_3)_3$ in D_2O on a deshielding scale. Saturation combs were applied prior to all repetition delays. All ^{27}Al MAS spectra were conducted using a single pulse excitation (1D) at a sample spinning frequency of 15 kHz. Typical 90° pulse lengths for the ^{27}Al central transition were 1.25 μs and recycle delays of 10.0 s.

2.5. *Tetrahydropyranylation of alcohols*

The catalytic tests were performed in the liquid phase under atmospheric pressure at room temperature in a multi-experiment workstation StarFish. Prior to the experiment, the catalyst (50 mg) was activated at 450 °C for 90 min with a rate of 10 °C min^{-1}. In a typical run, mesitylene (0.25 g, internal standard), 3,4-dihydro-2H-pyran (DHP, 15 ml, also as solvent) and the catalyst (50 mg) were placed in a two-necked vessel equipped with a condenser and a thermometer. Alcohol (i.e. 3,5,5-trimethylhexan-1-ol, tert-butanol, 2-cyclohexylethanol, 1-hexanol, 1-decanol or 1-hexadecanol, 18 mmol) was then added into the vessel. Samples of the reaction mixture were taken periodically and analyzed by using Agilent 6850 GC equipped a polar DB-WAX column (length 20 m, diameter 0.180 mm, and film thickness 0.3 μm) and flame ionization detector.

Turnover frequency was calculated based on following formula:

$$TOF = \frac{\mathrm{N\ x\ Con.\%}}{\mathrm{(CL + CB)\ x\ M\ x\ 2h}}$$

Where N stands for 18 mmol of alcohol, Con.% is the conversion after 2h, (CL+CB is the amount of catalytical sites based on pyridine adsorption followed by FTIR and M is the weight of the catalyst (50 mg).

To investigate if there is a leaching procedure happening during the reaction, a leaching test was performed with 9 mmol 2-cyclohexylethanol, 100 mg catalyst (DeSi1) and 10 ml DHP at 60 °C.

3. Results and discussion

3.1. Characterization of bulk and nanosponge MTW

Zeolite MTW was prepared in the form of bulk crystals and in the hierarchical form called nanosponge. Both materials have similar Si/Al molar ratio 52 and 54, respectively. Figure 1A shows the powder diffraction patterns of the bulk and nanosponge MTW. The latter material exhibits broader and less intense peaks due to its unique morphology (Fig. 2). The HRTEM images of the nanosponge material (Fig. 3 (4)) show the large agglomerations of nanocrystals of the size of 5 – 10 nm in average, similarly as it is reported in the literature [23, 24, 40]. Bulk MTW crystallizes as regular polycrystals of size about 1 – 1.5 μm in each dimension (Fig. 2). Closer examination of HRTEM images revealed that individual crystals are actually made of crystalline domains of approximately 200 – 500 nm (see Fig. 3 (1)). Bulk

MTW has BET area of 296 m^2/g and total pore volume of 0.224 cm^3/g (Table 1). Nanosponge MTW, on the other hand, has due to its unique nanocrystal arrangement consisting of randomly assembled thin crystallites with large empty volumes in interparticle space higher surface area of 454 m^2/g and three-time larger total pore volume, 0.716 cm^3/g. Also, FFT pattern confirms the polycrystallinity corresponding to the powder XRD pattern of nanosponge MTW, which shows less intense and wider peaks in comparison to the bulk and desilicated samples (Fig. 1).

Table 1

Si/Al molar ratio measured by the ICP/OES and textural properties of the MTW zeolite samples (desilicated materials from the 1st batch) determined by nitrogen sorption.

Material	Si/Al	BET [m^2/g]	S_{ext} [m^2/g]	V_{tot} [cm^3/g]	V_{mic} [cm^3/g]
Bulk MTW	52	296	55	0.224	0.103
DeSi1 MTW	45	80	62	0.245	0.008
DeSi2 MTW	45	80	64	0.348	0.006
DeSi3 MTW	42	236	126	0.382	0.057
Nanosponge MTW	54	454	288	0.716	0.070

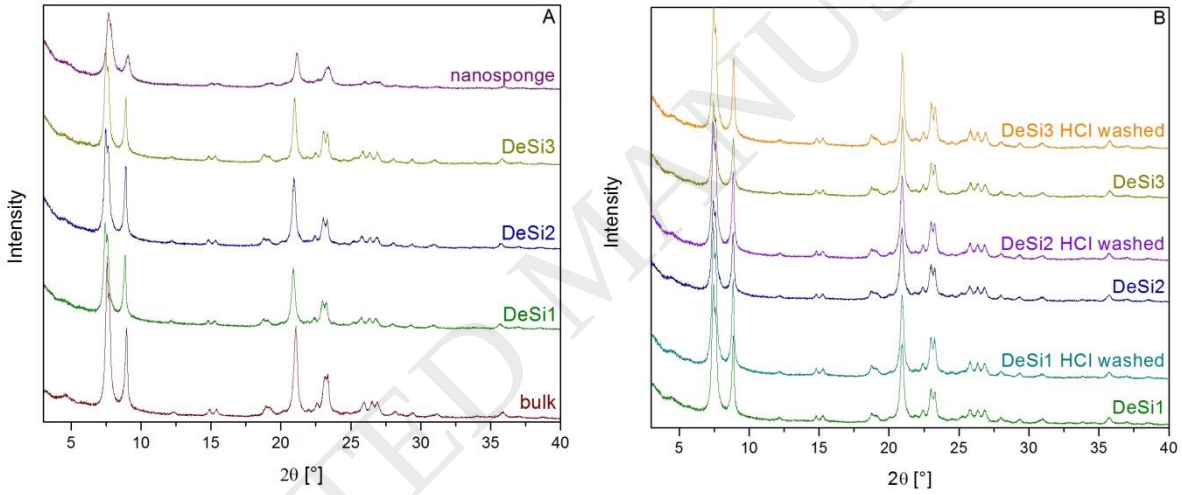

Fig. 1. Powder X-ray diffraction patterns of the MTW zeolite samples, desilicated MTW from the 1st batch (A) and the 2nd batch (B).

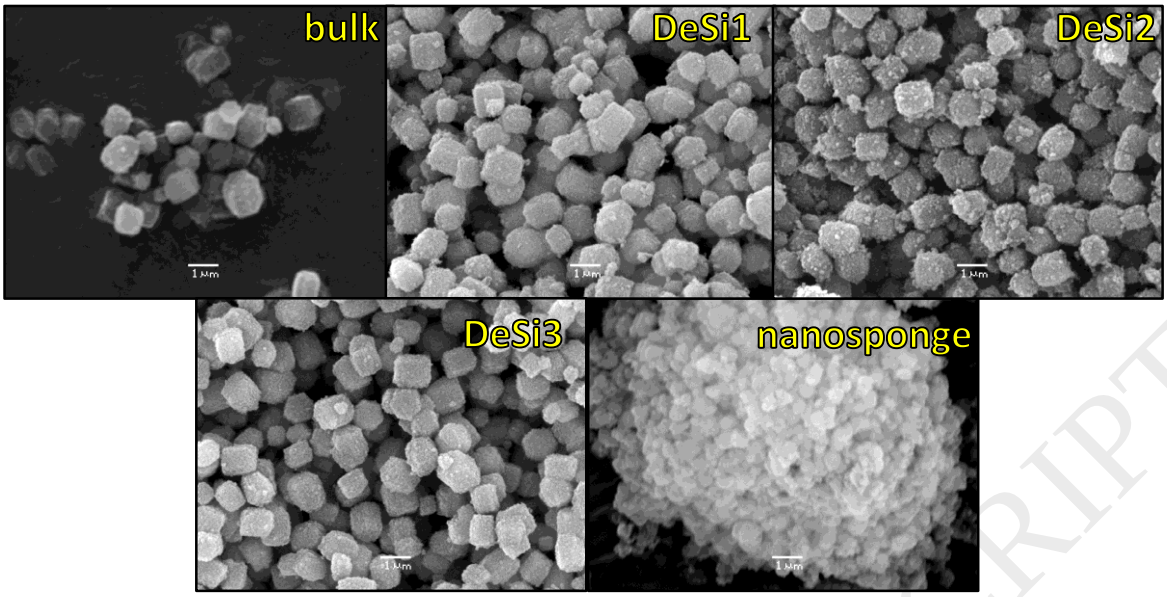

Fig. 2. SEM images of the MTW bulk and nanosponge samples and desilicated materials from the 1st batch.

The acidic properties were evaluated based on FTIR spectra using pyridine and DTBPy as probe molecules (Fig. 4). The most intense band for both the bulk and nanosponge sample is at 3744 cm^{-1} typically assigned to terminal silanol groups. The band is most intensive in case of the nanosponge MTW due to its large external surface area compared to the bulk MTW sample. In the case of bulk MTW, the band at 3744 cm^{-1} has a tail towards lower frequencies. This band is associated with internal silanols and suggests the presence of defects in bulk crystals [42, 43]. Band at 3610 cm^{-1} clearly seen in both bulk and nanosponge material is unambiguously assigned to Si-(OH)-Al bridging hydroxyl groups. Another less intensive band at 3575 cm^{-1} follows. Its assignment is not conclusive despite the fact that it has been reported for MTW materials in few cases [15, 43-45]. Due to its close wavenumber to typical bridging hydroxyls the band in this region is attributed by most researchers to a second kind of bridging hydroxyls. Two types of Si-(OH)-Al groups is not unusual and it is characterized for instance for zeolites FAU and MOR [42]. After the adsorption of pyridine both bridging hydroxyl bands disappear both in the case of bulk and nanosponge material. It demonstrates good accessibility of both sites for pyridine molecule. As the Table 2 shows the bulk MTW contains more Brønsted-type acid sites, 0.111 mmol/g, than the Lewis-type, 0.027 mmol/g. Furthermore, as little as one third of the Brønsted sites are accessible for larger DTBPy molecules (spectra not shown here). On the other hand, in the nanosponge MTW Lewis acid sites prevails over Brønsted (0.064 and 0.046 mmol/g, respectively), however, all Brønsted sites are accessible for bulk DTBPy molecules. The good accessibility to acid centres even for bulky probe/reactant molecules is a typical feature of nanosponge-like morphology and their main advantage [23, 24, 40].

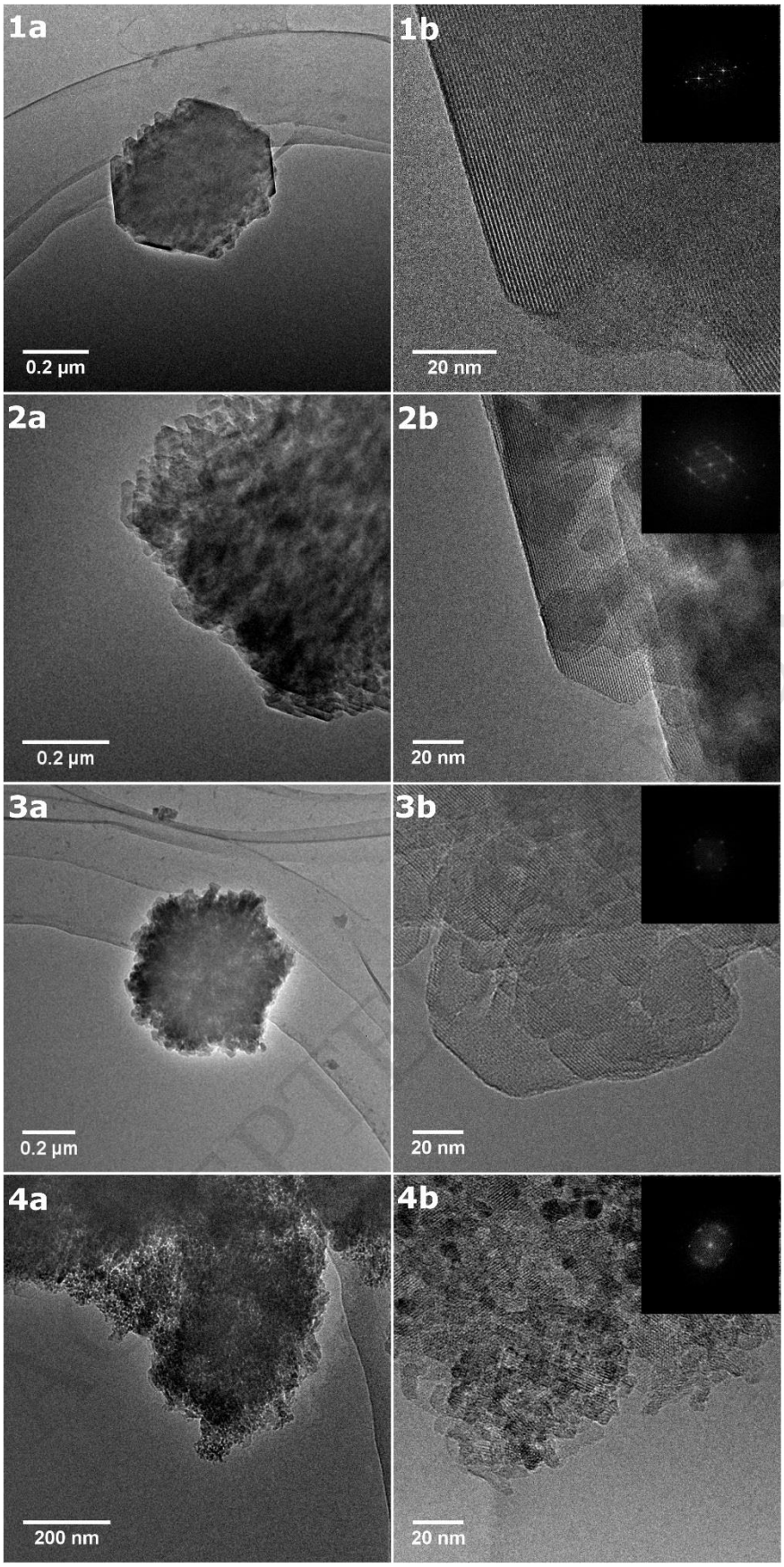

Fig. 3. HRTEM images of the bulk MTW (1a,b), DeSi1 (2a,b), DeSi1 HCl washed (3a,b) and nanosponge MTW (4a,b) samples.

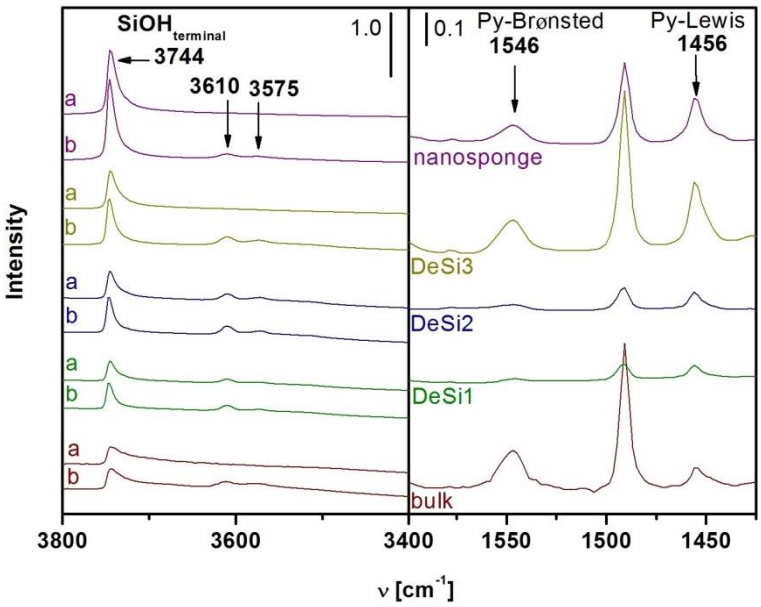

Fig. 4. FTIR spectra of the MTW zeolite samples (bulk, nanosponge and desilicated from the 1st batch); region of hydroxyl vibration (left side) and region of pyridine vibration (right side); *b* – before the adsorption of pyridine, *a* - after the adsorption of pyridine at 150 °C.

3.2. Effect of desilication in the presence of tetraalkylammonium cations

To introduce additional mesoporosity into bulk MTW crystals, parent material was desilicated using three types of solutions (DeSi1 = TPA-OH + NaOH, DeSi2 = TBA-OH + NaOH and DeSi3 = NaOH). After the first desilication, in so called 1st batch, we can observe slight decrease of the diffraction intensities (Fig. 1A) as a result of a structural damage of a small scale. According to SEM images (Fig. 2) the desilication procedure did not significantly change the crystallinity of material, however, the surface of crystals is obviously rougher after desilication. Adsorption isotherms of the desilicated samples (the 1st batch) in Fig. 5 demonstrate a significant decrease in the total surface area and the micropore volume for the DeSi1 and DeSi2 samples, *i.e.* after desilication with tetraalkylammonium-containing solutions (Table 1). This would be expected with samples that were not calcined and the TAA^+ ions block the entrances to micropores. However, here the micropore volume remains limited even after the calcination. It implies that the blocking particles are not of an organic origin but could be composed of the inorganic remnants of the crystal framework, destroyed during the desilication.

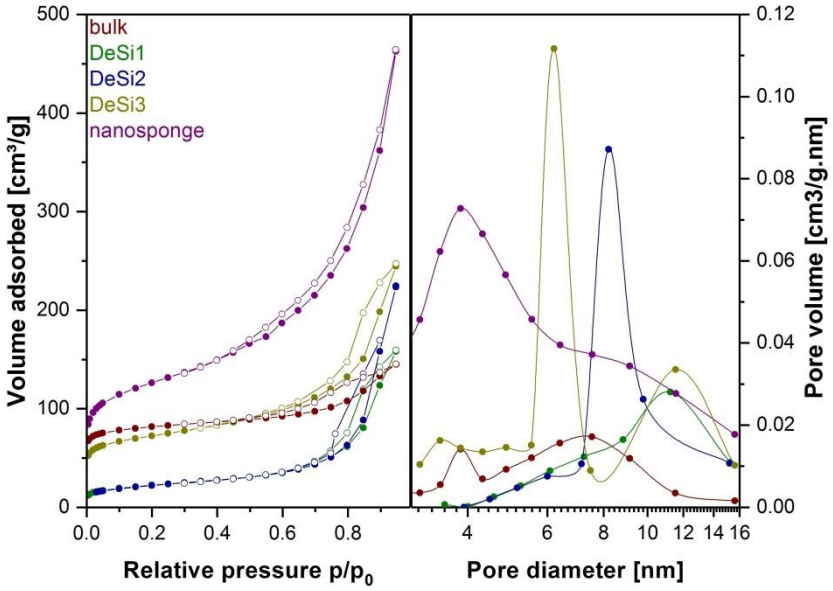

Fig. 5. Adsorption isotherms and pore size distributions of the MTW bulk, nanosponge and desilicated materials from the1st batch. The pore size distribution was determined using the BJH model from the desorption branch of the isotherms.

FTIR spectra of the 1st batch desilicated samples also support the previous assumption (Fig. 4). The intensity of the bands for pyridine adsorbed on acid sites and thus the concentration of both types of acid sites pronouncedly decreased upon desilication with TAA^+ solutions (DeSi1 and DeSi2). Moreover, the bands attributed to bridging hydroxyl groups at 3610 cm^{-1} and 3575 cm^{-1} remain visible after the pyridine adsorption proving that some acid sites are not accessible for the pyridine. The FTIR results correspond to the results from nitrogen sorption and indicates the micropore blockage in the cases when TAA^+ solutions where used for desilication. Conversely, material desilicated with pure NaOH solution, DeSi3, exhibits larger external surface area and higher total pore volume compared to bulk parent MTW (Table 1). The micropore volume decrease is explained by uncontrolled desilication and formation of mesopores on expense of micropores [15]. ^{27}Al MAS NMR analysis of the desilicated samples (in Supplementary Information Fig. S1) shows an intense band of tetrahedrally coordinated aluminium at 60 ppm for all three DeSi materials. Nevertheless, in spectra of the DeSi1 and DeSi2 another signal at 0 ppm is present. This one in particular proves the presence of octahedrally coordinated aluminium, the suggesting presence of extraframework material originating from destroyed framework. A small signal in this region is also visible in DeSi3 sample spectra, however, its low intensity compared to DeSi1 and DeSi2 implies that if the extraframework material was formed during the desilication, it was rather washed out than remain and block the micropores. These findings are in agreement with sorption and FTIR data and it corresponds to results previously reported for desilication of MTW with NaOH solutions [15].

Table 2
Acidic properties of the MTW materials based on pyridine and DTBPy adsorption followed by FTIR.

Type of material		Pyridine			DTBPy
		c_{Lewis} [mmol/g]	$c_{Brønsted}$ [mmol/g]	$c_L + c_B$ [mmol/g]	$c_{Brønsted}$ [mmol/g]
Bulk		0.027	0.111	0.138	0.033
Nanosponge		0.064	0.046	0.110	0.054
1st batch	DeSi1	0.017	0.011	0.028	n.d.
	DeSi2	0.022	0.013	0.035	n.d.
	DeSi3	0.088	0.088	0.176	n.d.
2nd batch	DeSi1	0.032	0.048	0.080	n.d.
	DeSi1 HCl washed	0.073	0.125	0.198	0.101
	DeSi2	0.028	0.029	0.057	0.000
	DeSi2 HCl washed	0.049	0.075	0.124	n.d.
	DeSi3	0.147	0.165	0.312	n.d.
	DeSi3 HCl washed	0.055	0.076	0.131	0.074

n.d. – not determined due to a small amount of the sample

3.3. Additional acid washing of desilicated materials

The obvious micropore blockage is surprising phenomena as the presence of TAA^+ shall act as surface protecting agent and on the contrary it shall support the creation of mesopores inside bulk crystals [16]. In order to overcome the problem of micropore blockage, the second batch of desilicated samples was prepared by the same procedure. Each sample was split in half and half of each sample was treated with 0.1 M hydrochloric acid prior to calcination. Comparison of the 1st and 2nd batch of desilicated materials show reasonable agreement taking in account the fact that reproducibility of desilication is always little bit tricky. As a benchmark for our two batches we chose comparison of textural properties (Table 1 and Table 3) because the FTIR data (values obtain from pyridine sorption) are distorted by inaccessibility of some acid sites. Still, FTIR spectra (Fig. 6) show the same phenomena for DeSi1 and DeSi2 which contain acid sites not accessible for pyridine while DeSi3 acid sites can be fully occupied by pyridine.

Almost identical XRD diffraction patterns of washed and unwashed samples (Fig. 1B) indicate the structural integrity and resistance to the additional acid washing. The polycrystals of desilicated materials were after the HCl treatment of the same size (1-1.5 μm) (see SEM images in Fig. 7), however, the domains were significantly smaller (10-50 nm) (exemplified on DeSi1 HRTEM images in Fig. 3 before (2) and after (3) HCl washing). The confirmation of this is shown in the FFT diffraction patterns merged in the images in the Fig 3. Also, the STEM images show the difference between the bulk MTW and after its desilication with TPAOH+NaOH solution (DeSi1) and additional HCl washing (Fig. 8). It evidence homogeneously distributed mesopores while the crystal size and shape remained largely unaffected. After the acid washing we observe a significant increase of the micropore volume in DeSi1 (5-times) and DeSi2 (7-times) reaching almost original values in the parent bulk material (Fig. 9, Table 3). The micropore release is accompanied by the increase of the total surface area, the external surface area and the total pore volume reaching similar or even higher values like DeSi3 material desilicated only with pure NaOH.

Table 3

Comparison of textural properties and Si/Al ratio (measured by SEM-EDS) of the desilicated MTW zeolite samples before and after HCl washing (the 2nd batch).

Material	BET [m^2/g]	S_{ext} [m^2/g]	V_{tot} [cm^3/g]	V_{mic} [cm^3/g]	Si/Al
DeSi1	113	65	0.229	0.020	35
DeSi1 HCl washed	380	126	0.345	0.108	44
DeSi2	87	57	0.253	0.013	37
DeSi2 HCl washed	338	121	0.362	0.092	32
DeSi3	278	113	0.329	0.070	28
DeSi3 HCl washed	327	131	0.384	0.083	36

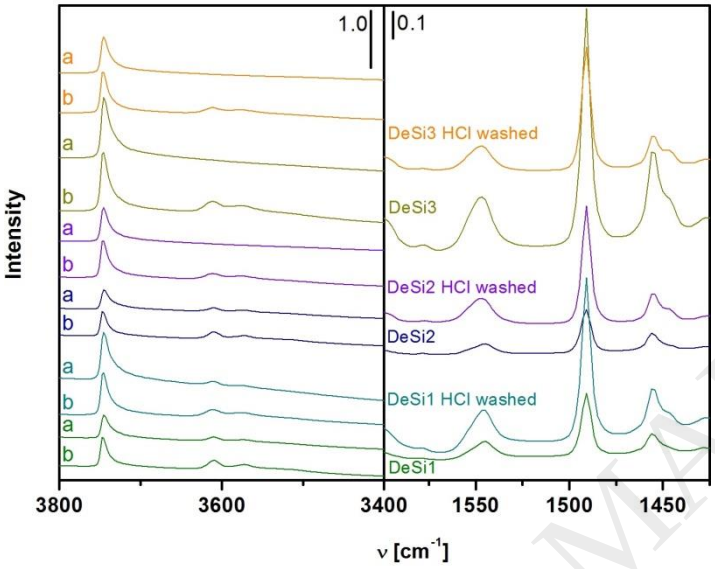

Fig. 6. FTIR spectra of the desilicated MTW zeolite samples with and without acid washing;); region of hydroxyl vibration (left side) and region of pyridine vibration (right side); *b* – before the adsorption of pyridine, *a* - after the adsorption of pyridine at 150 °C.

The acid treatment obviously increased the accessible volume of micropores and thus the detected concentration of acid sites in DeSi1 and DeSi2 (Table 2). After the acid washing the bands of bridging hydroxyl groups completely disappeared after pyridine adsorption only in the case of DeSi2 while it remains partially visible for DeSi1 (Fig. 6). One may suggest that some acid sites are still not accessible as the micropore unblocking was not completed. In DeSi3 material (desilicated with pure NaOH solution) the concentration of acid sites decreased after the acid treatment, probably due to the dealumination. The dealumination process is expected as the whole porous system is open, while in the case of DeSi1 and DeSi2 the micropores should be unblocked first and then the dealumination can proceed. Keeping the same time of the acid treatment the dealumination procedure in DeSi1 and DeSi2 did not probably start up or proceed in little extent compared to open system of DeSi3. The Si/Al molar ratios determined by SEM-EDS (Table 3, Fig. S2) generally decreased for all desilicated samples, which is reasonable as silicon and partially also aluminium atoms (especially in the case DeSi3) are removed from the framework. Nonetheless, based on comparison of the elemental maps (STEM-EDS) of bulk MTW and DeSi1 after HCl washing we can conclude that the aluminium distribution has not been significantly changed (see Fig. S3 and Fig. S4).

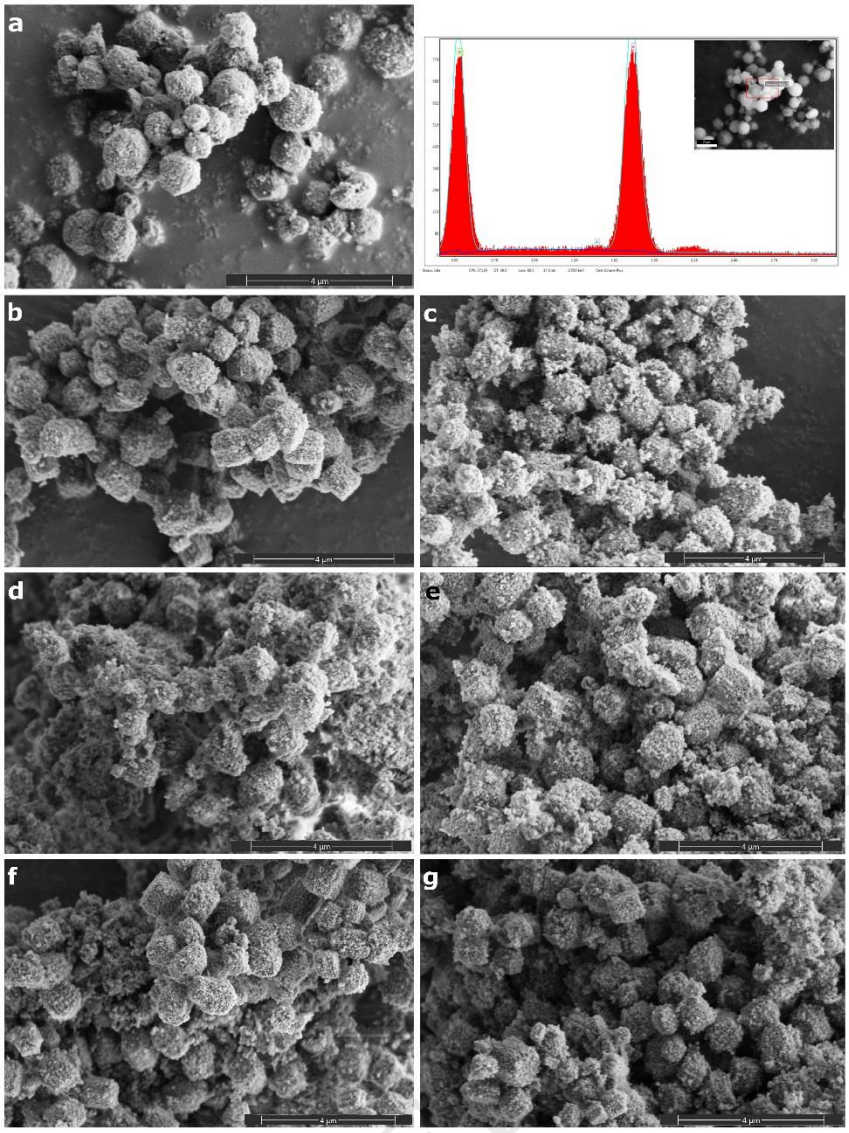

Fig. 7. SEM images of bulk MTW (a), DeSi1 (b), DeSi1 HCl washed (c), DeSi2 (d), DeSi2 HCl washed (e), DeSi3 (f), and DeSi3 HCl washed (g) materials with example of EDS spectrum (top right) for bulk MTW (determined Si/Al is 46). Desilicated and washed materials are from the 2nd batch. The internal scale for each image is 4 μm).

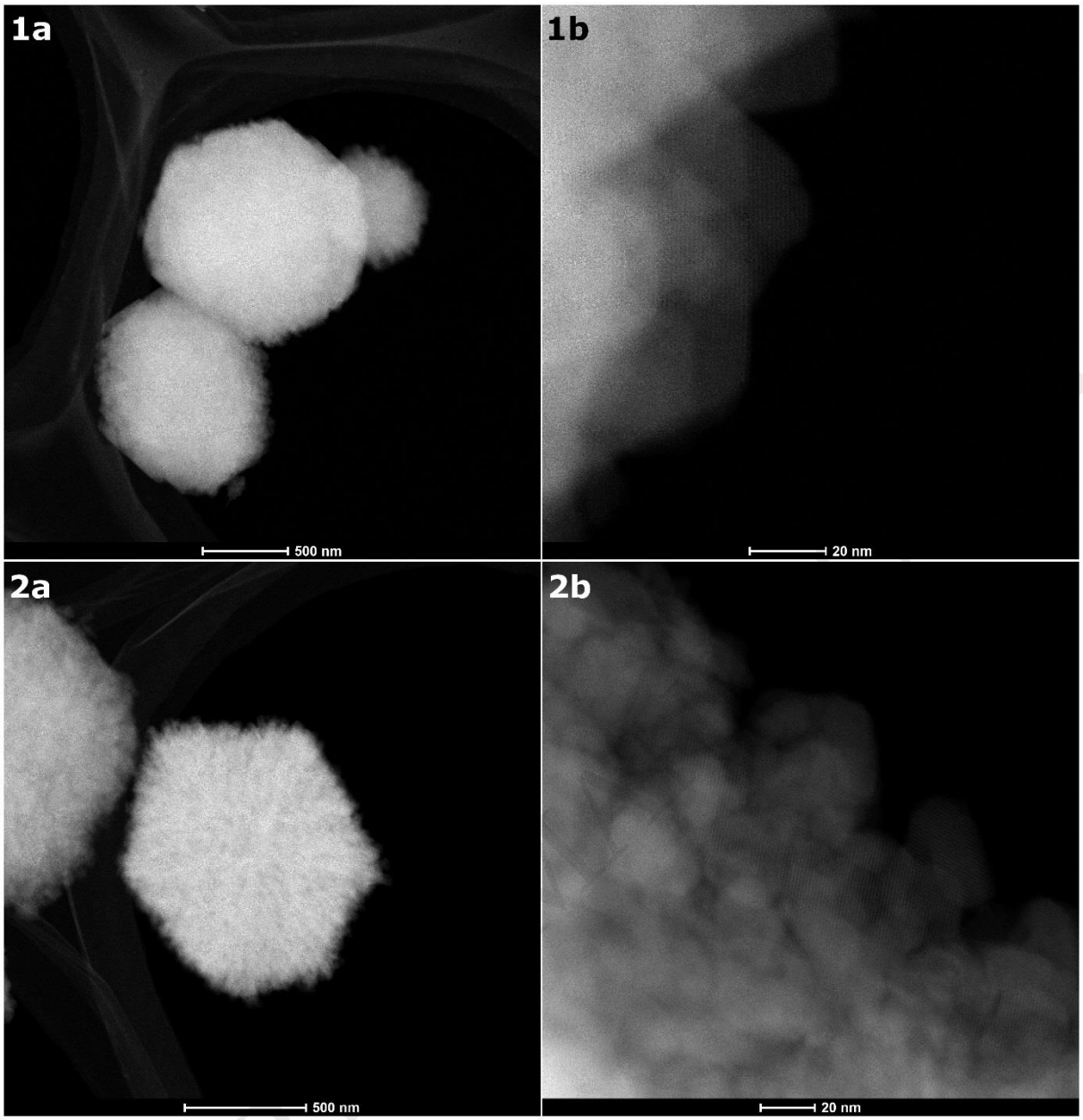

Fig. 8. STEM images of bulk MTW (1a,b) and DeSi1 HCl washed (2a,b) samples.

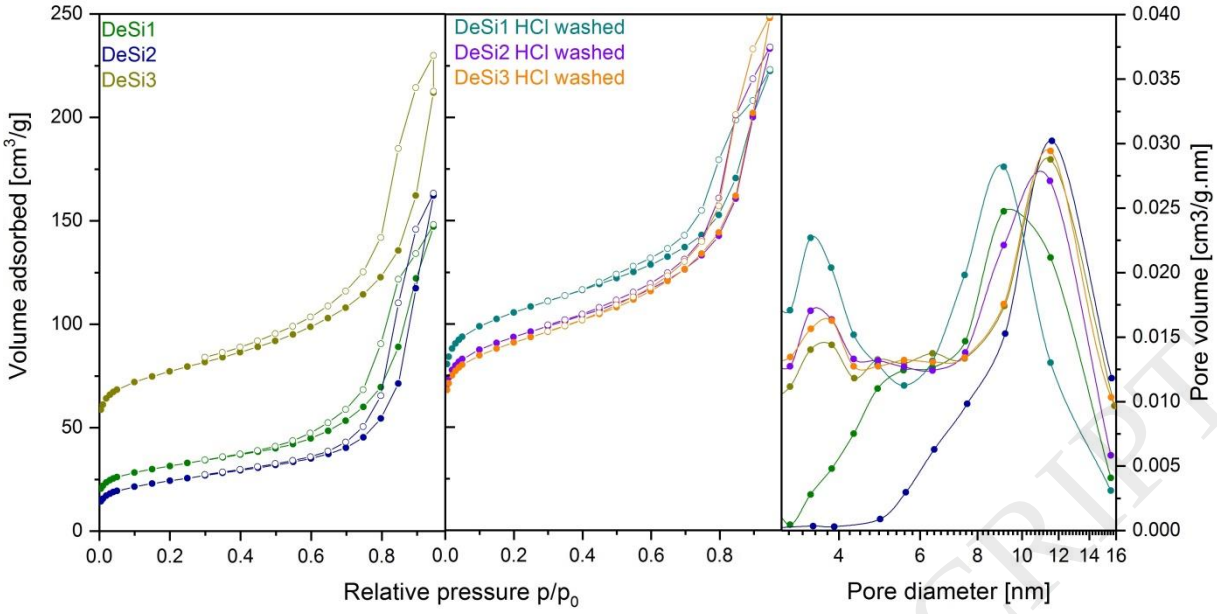

Fig. 9. Comparison of the adsorption isotherms and pore size distributions of the desilicated MTW zeolite samples with and without acid washing. The pore size distribution was determined using the BJH model from the desorption branch of the isotherms.

3.4. Catalysis

The activity of desilicated and nanosponge MTW materials was evaluated in the tetrahydropyranylation of two sets of alcohols: i) linear primary alcohols assumed to have similar intrinsic activity of hydroxyl group but significantly different length of carbon chains (molecules with C_6, C_{10} and C_{16} backbones), and ii) branched alcohols with branching at γ- (acyclic 3,5,5-trimethylhexan-1-ol possessing relatively bulk tail-group and 2-cyclohexylethanol with similar size of the molecule but having cyclic group) and α-positions (t-butanol). Since the reaction under study can proceed over both Brønsted and Lewis acid sites [40], the comparison of the catalysts activity (turnover frequency values, TOF) was done using the total concentration of active sites in respective materials (Table 2, we assume that acid sites not accessible for pyridine are not accessible for reactants as well, therefore we used the number of acid sites quantified by pyridine FTIR method). In the tetrahydropyranylation reaction involving 1-hexanol, 1-decanol, and 1-hexadecanol, most of the catalysts reach the maximal conversions (plateau) after 6 h of reaction time (Fig. 10). In the case of nanosponge MTW zeolite, this plateau was caused by the total consumption of the reactant (100 % conversion of 1-hexanol and 1-decanol after 6 h, Fig. 10), while the significant decrease in the reaction rate at the conversions < 50 % for majority of desilicated samples can be explained by partial deactivation of their active sites.

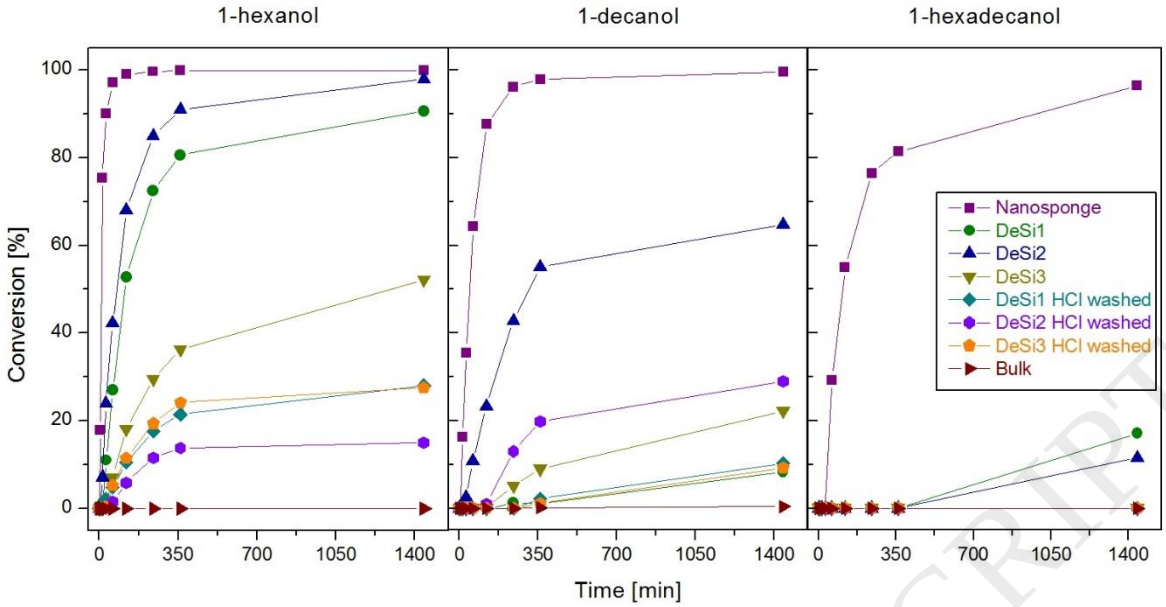

Fig. 10. Conversion of tetrahydropyranylation of 1-hexanol (A), 1-decanol (B), and 1-hexadecanol (C) (50 mg of catalyst + 15 ml DHP + 18 mmol of alcohol, at room temperature).

When the smallest non-branched primary alcohol (1-hexanol) was used as the reactant, activities of nanosponge MTW and those obtained by desilication in the presence of TAA^+ cations (DeSi1 and DeSi2) were comparable (Fig. 10). Taking into account relatively low concentration of active sites accessible in DeSi2 sample, the TOF value for this material was even higher in comparison with nanosponge analogue (Fig. 11). The results of 1-hexanol tetrahydropyranylation indicate that in the case of desilicated materials, despite the blockage of the micropores, reaction can be efficiently catalysed by the acid sites located on the external surface of the crystals. In order to understand if mentioned sites can be considered as really external (accessible for bulky molecules) or just as sites located in micropore (or small mesopore) mouths, medium- (1-decanol) and large-size (1-hexadecanol) alcohols were used as reactants. As it was expected, activity of nanosponge MTW gradually decreased with increase in number of carbon atoms in the molecule of linear alcohol used: TOF values changed in the order 1650 h^{-1} (1-hexanol), 1400 h^{-1} (1-decanol), and 850 h^{-1} (1-hexadecanol), respectively. With increase of the molecule size (especially for 1-hexadecanol) the activity of desilicated samples dramatically decreased (Fig. 11) indicating that respective sites have moderate accessibility in comparison with nanosponge and bulk analogues. While the active sites of former material are accessible for all alcohols under study including the most bulky 1-hexadecanol, the latter zeolite exhibited negligible conversions even of the smallest 1-hexanol (Fig. 10, 11).

Unexpectedly, after the liberation of micropores by the treatment with HCl solution, both conversions and activities (TOF) achieved for desilicated samples were significantly lower in comparison with those obtained for materials with blocked channels (Fig. 10, 11). This observation can be explained by the high diffusional constraints for reactants as well as for products of tetrahydropyranylation reaction in the one-dimensional pore system of MTW. Despite the higher values of all textural parameters (V_{micro}, V_{total}, S_{BET}, S_{ext}) achieved for the samples after washing with HCl solution, released micropore space (and created mesopores) can act as a trap for participating molecules. Free micropores of one-dimensional channel present long diffusion path of the reactant/product molecules through the crystal and thus the reaction rate is decreased. Therefore the micropores in MTW should be considered as a negative factor affecting the catalytic activity.

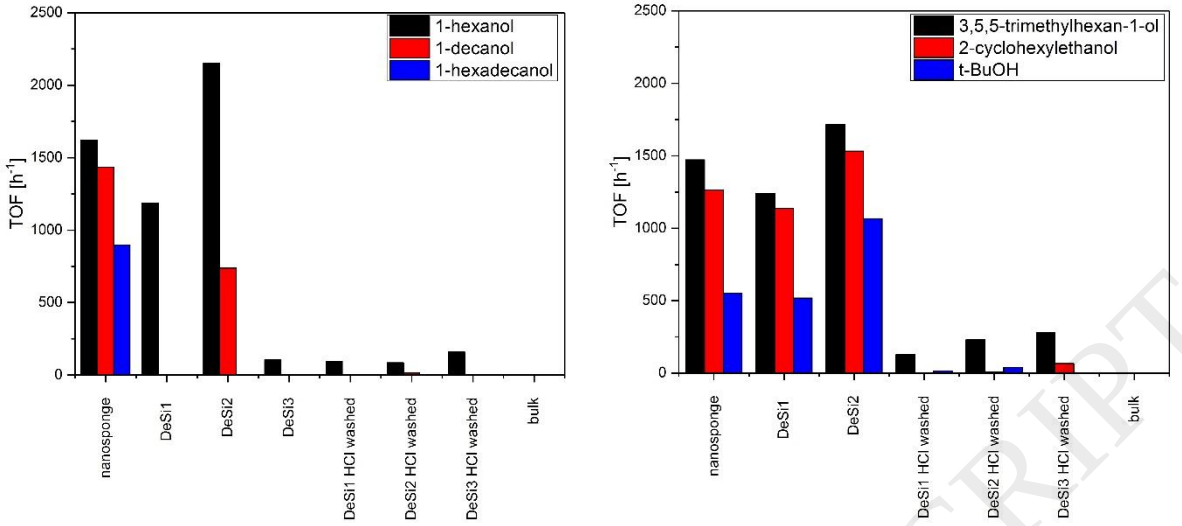

Fig. 11. TOF in the reaction of linear primary alcohols (on the left) and branched alcohols (on the right) with DHP after 2h.

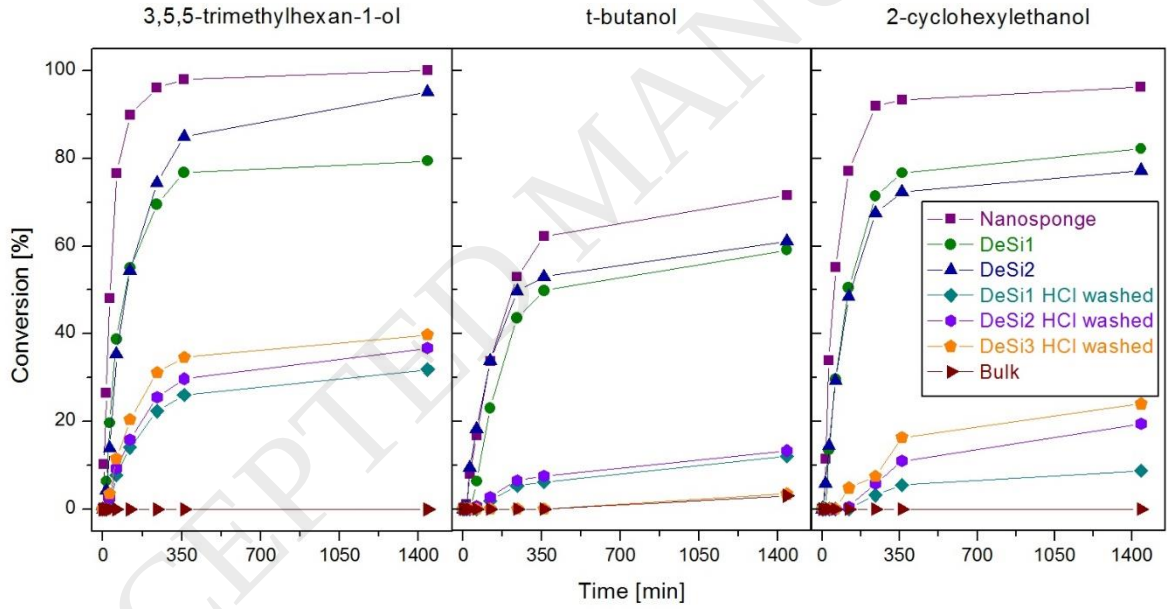

Fig. 12. Conversion of particular alcohol in tetrahydropyranylation reaction of 1-hexanol (A), 1-decanol (B), and 1-hexadecanol (C) (50 mg of catalyst + 15 ml DHP + 18 mmol of alcohol, at room temperature).

In contrast to tetrahydropyranylation of linear non-branched alcohols, desilicated samples prepared the presence of TAA^+ cations (DeSi1 and DeSi2) exhibited reasonable activities in transformation of branched primary and tertiary alcohols (Fig. 11, 12). It is worth to underline, that TOF values calculated for reactions over DeSi2 material exceeded those for nanosponge zeolite independently on the type of reagent (3,5,5-trimethylhexan-1-ol, 2-cyclohexylmethanol, t-butanol). DeSi1 material exhibits only slightly lower TOF values for all three alcohols compared to nanosponge. Removal of the solid deposits from the micropores again leads to the significant drop in the catalyst activity. We believe that the origin of the low activity of DeSi3 sample and materials obtained after additional treatment with HCl is the

same – a high fraction of micropores and mesopores in bulk crystal. This resulted in the long diffusion paths of reactants/products through hierarchically porous but bulk crystal. On the contrary in nanosponge MTW the reaction probably proceeds in the mesopore space between nanosized crystals, which significantly facilitates the reaction. In the case of DeSi1 and DeSi2 the reaction takes place on the external surface of crystals or in micropores but close to the pore openings.

To confirm the heterogeneity of the reactions over MTW materials studied, the leaching test was performed. After separation of the catalyst from the reaction mixture by hot filtration and centrifugation (details in Experimental part), no further increase of the alcohol conversion was observed (results are not shown). This indicates the absence of the leaching of active sites from zeolite framework during the tetrahydropyranylation reaction under the conditions used.

4. Conclusions

All above discussed results lead us to following summary and conclusions about top-down desilication of MTW and its comparison with bottom-up synthesized nanosponge.

Desilication of MTW zeolite in the presence of TAA^+ cations have a different pattern compared to MFI reported in the literature. The distinct process is attributed to the different dimensionality of channel system in MTW and MFI zeolite, one-dimensional vs. three-dimensional. In the case of MTW, when TAA^+ interacts with the crystal surface, it may also block the openings of the one-dimensional channels. As a result, the desilication in the crystal can be obstructed and the structural debris can hardly diffuse out from the crystal, thus blocking the micropores and restricting the access to created mesopores. Created micropores and mesopores can be released by acid treatment without observation of the dealumination effect. When the material desilicated with pure NaOH solution (DeSi3) was acid treated, the partial dealumination was confirmed.

The liberation of micro- and mesopores turned out to be not as beneficial as expected. In all studied catalytic reactions, the materials desilicated in the presence of TAA^+ cations (with blocked pores) exhibited significantly higher activity compared to their acid washed counterparts (with released pore system), material desilicated only with NaOH solution and bulk MTW (parent material). We hypothesize that a high fraction of micro- and mesopores in bulk crystal (1 – 1.5 μm) results in the limited mass transfer of reactants/products. This effect is particularly demonstrated in the reaction with branched alcohols. Nanosponge, on the other hand, represents agglomerations of nanocrystals of the size of 5 – 10 nm with large void volumes in the interparticle space. Among studied materials it exhibits the highest catalytic activity in terms of TOF values when long non-branched alcohols are involved (1-decanol, 1-hexadecanol). In the reaction of branched alcohols, the catalytic activity of MTW desilicated in the presence of TBA^+ cation (DeSi2) overcome nanosponge MTW when comparing TOF values. Despite the pore-blocking phenomena observed with desilication using TAA^+ we prepared materials possessing comparable or even better catalytic activity with nanosponge MTW.

Acknowledgment

Authors thank the Czech Science Foundation for financial support (17-06524Y). H.P. and J.Y. thank to the 111 project of the Ministry of Education of China (B17020). M.M. and S.M.V. acknowledge the support of EPSRC grant EP/K025112/1 and Capital for Great Technologies Grant EP/L017008/1. Authors thank to Valeryia Kasneryk and Martin Hartmann for measurement of solid state ^{27}Al NMR at Friedrich-Alexander-Universität Erlangen-Nürnberg.

References

[1] J. Čejka, H. van Bekkum, A. Corma, F. Schueth, Introduction to Zeolite Molecular Sieves, Elsevier, Amsterdam, 2007.
[2] W. Vermeiren, J.P. Gilson, Impact of zeolites on the petroleum and petrochemical industry, Topics in Catalysis, 52 (2009) 1131-1161.
[3] D. Kubička, I. Kubičková, J. Čejka, Application of Molecular Sieves in Transformations of Biomass and Biomass-Derived Feedstocks, Catalysis Reviews, 55 (2013) 1-78.
[4] J. Čejka, E.R. Morris, P. Nachtigall, Zeolites in Catalysis: Properties and Applications, The Royal Society of Chemistry2017.
[5] A. Corma, From microporous to mesoporous molecular sieve materials and their use in catalysis, Chemical Reviews, 97 (1997) 2373-2419.
[6] W.J. Roth, P. Nachtigall, R.E. Morris, J. Čejka, Two-Dimensional Zeolites: Current Status and Perspectives, Chemical Reviews, 114 (2014) 4807-4837.
[7] P. Eliasova, M. Opanasenko, P.S. Wheatley, M. Shamzhy, M. Mazur, P. Nachtigall, W.J. Roth, R.E. Morris, J. Cejka, The ADOR mechanism for the synthesis of new zeolites, Chemical Society Reviews, 44 (2015) 7177-7206.
[8] M.V. Opanasenko, W.J. Roth, J. Cejka, Two-dimensional zeolites in catalysis: current status and perspectives, Catalysis Science & Technology, 6 (2016) 2467-2484.
[9] O. Masaru, S. Shin-ya, T. Junko, N. Yasuto, K. Eiichi, M. Masahiko, Formation of Uniform Mesopores in ZSM-5 Zeolite through Treatment in Alkaline Solution, Chemistry Letters, 29 (2000) 882-883.
[10] J.C. Groen, J.A. Moulijn, J. Pérez-Ramírez, Decoupling mesoporosity formation and acidity modification in ZSM-5 zeolites by sequential desilication–dealumination, Microporous and Mesoporous Materials, 87 (2005) 153-161.
[11] J. Perez-Ramirez, C.H. Christensen, K. Egeblad, C.H. Christensen, J.C. Groen, Hierarchical zeolites: enhanced utilisation of microporous crystals in catalysis by advances in materials design, Chemical Society Reviews, 37 (2008) 2530-2542.
[12] M. Kubů, M. Opanasenko, D. Vitvarová, Desilication of SSZ-33 zeolite – Post-synthesis modification of textural and acidic properties, Catalysis Today, 243 (2015) 46-52.
[13] M. Kubů, N. Žilková, J. Čejka, Post-synthesis modification of TUN zeolite: Textural, acidic and catalytic properties, Catalysis Today, 168 (2011) 63-70.
[14] M. Kubů, M. Opanasenko, M. Shamzy, Modification of textural and acidic properties of -SVR zeolite by desilication, Catalysis Today, 227 (2014) 26-32.
[15] B. Gil, Ł. Mokrzycki, B. Sulikowski, Z. Olejniczak, S. Walas, Desilication of ZSM-5 and ZSM-12 zeolites: Impact on textural, acidic and catalytic properties, Catalysis Today, 152 (2010) 24-32.
[16] J. Pérez-Ramírez, D. Verboekend, A. Bonilla, S. Abelló, Zeolite Catalysts with Tunable Hierarchy Factor by Pore-Growth Moderators, Advanced Functional Materials, 19 (2009) 3972-3979.
[17] X. Li, D.F. Shantz, PFG NMR Investigations of Tetraalkylammonium−Silica Mixtures, The Journal of Physical Chemistry C, 114 (2010) 8449-8458.
[18] D. Verboekend, J. Perez-Ramirez, Desilication Mechanism Revisited: Highly Mesoporous All-Silica Zeolites Enabled Through Pore-Directing Agents, Chemistry-a European Journal, 17 (2011) 1137-1147.
[19] C.J.H. Jacobsen, C. Madsen, J. Houzvicka, I. Schmidt, A. Carlsson, Mesoporous Zeolite Single Crystals, Journal of the American Chemical Society, 122 (2000) 7116-7117.
[20] I. Schmidt, A. Boisen, E. Gustavsson, K. Ståhl, S. Pehrson, S. Dahl, A. Carlsson, C.J.H. Jacobsen, Carbon Nanotube Templated Growth of Mesoporous Zeolite Single Crystals, Chemistry of Materials, 13 (2001) 4416-4418.
[21] M. Choi, K. Na, J. Kim, Y. Sakamoto, O. Terasaki, R. Ryoo, Stable single-unit-cell nanosheets of zeolite MFI as active and long-lived catalysts, Nature, 461 (2009) 246-U120.
[22] J. Kim, W. Park, R. Ryoo, Surfactant-Directed Zeolite Nanosheets: A High-Performance Catalyst for Gas-Phase Beckmann Rearrangement, ACS Catalysis, 1 (2011) 337-341.

[23] J.-C. Kim, K. Cho, R. Ryoo, High catalytic performance of surfactant-directed nanocrystalline zeolites for liquid-phase Friedel–Crafts alkylation of benzene due to external surfaces, Applied Catalysis A: General, 470 (2014) 420-426.
[24] W. Kim, J.-C. Kim, J. Kim, Y. Seo, R. Ryoo, External Surface Catalytic Sites of Surfactant-Tailored Nanomorphic Zeolites for Benzene Isopropylation to Cumene, ACS Catalysis, 3 (2013) 192-195.
[25] P. del Campo, P. Beato, F. Rey, M.T. Navarro, U. Olsbye, K.P. Lillerud, S. Svelle, Influence of post-synthetic modifications on the composition, acidity and textural properties of ZSM-22 zeolite, Catalysis Today, 299 (2018) 120-134.
[26] S. Fernandez, M.L. Ostraat, J.A. Lawrence, K. Zhang, Tailoring the hierarchical architecture of beta zeolites using base leaching and pore-directing agents, Microporous and Mesoporous Materials, 263 (2018) 201-209.
[27] A. Katovic, B.H. Chiche, F. Di Renzo, G. Giordano, F. Fajula, Influence of the aluminium content on the acidity and catalytic activity of MTW-type zeolites, in: A. Corma, F.V. Melo, S. Mendioroz, J.L.G. Fierro (Eds.) Studies in Surface Science and Catalysis, Elsevier2000, pp. 857-862.
[28] B.H. Chiche, R. Dutartre, F. Di Renzo, F. Fajula, A. Katovic, A. Regina, G. Giordano, Study of the sorption and acidic properties of MTW-type zeolite, Catalysis Letters, 31 (1995) 359-366.
[29] C.W. Jones, S.I. Zones, M. E. Davis, m-Xylene reactions over zeolites with unidimensional pore systems, Applied Catalysis A: General, 181 (1999) 289-303.
[30] W. Zhang, P.G. Smirniotis, On the exceptional time-on-stream stability of HZSM-12 zeolite: relation between zeolite pore structure and activity, Catalysis Letters, 60 (1999) 223-228.
[31] W. Zhang, P.G. Smirniotis, Effect of Zeolite Structure and Acidity on the Product Selectivity and Reaction Mechanism forn-Octane Hydroisomerization and Hydrocracking, Journal of Catalysis, 182 (1999) 400-416.
[32] K. Yoo, E.C. Burckle, P.G. Smirniotis, Comparison of protonated zeolites with various dimensionalities for the liquid phase alkylation of i-butane with 2-butene, Catalysis Letters, 74 (2001) 85-90.
[33] S. Gopal, P.G. Smirniotis, Deactivation Behavior of Bifunctional Pt/H-Zeolite Catalysts during Cyclopentane Hydroconversion, Journal of Catalysis, 205 (2002) 231-243.
[34] J. Weitkamp, S. Ernst, R. Kumar, The spaciousness index: A novel test reaction for characterizing the effective pore width of bifunctional zeolite catalysts, Applied Catalysis, 27 (1986) 207-210.
[35] E.T.C. Vogt, G.T. Whiting, A. Dutta Chowdhury, B.M. Weckhuysen, Chapter Two - Zeolites and Zeotypes for Oil and Gas Conversion, in: F.C. Jentoft (Ed.) Advances in Catalysis, Academic Press2015, pp. 143-314.
[36] T.W. Greene, P.G.M. Wuts, Protection for the Hydroxyl Group, Including 1,2- and 1,3-Diols, Protective Groups in Organic Synthesis, John Wiley & Sons, Inc.2002, pp. 17-245.
[37] B. Tamami, K. Parvanak Borujeny, Chemoselective tetrahydropyranylation of alcohols and phenols using polystyrene supported aluminium chloride as a catalyst, Tetrahedron Letters, 45 (2004) 715-718.
[38] G.P. Romanelli, G. Baronetti, H.J. Thomas, J.C. Autino, Efficient method for tetrahydropyranylation/depyranylation of phenols and alcohols using a solid acid catalyst with Wells–Dawson structure, Tetrahedron Letters, 43 (2002) 7589-7591.
[39] A. Hegedüs, I. Vígh, Z. Hell, Zeolite- Catalyzed Environmentally Friendly Tetrahydropyranylation of Alcohols and Phenols, Synthetic Communications, 34 (2004) 4145-4152.
[40] H.S. Shin, M. Opanasenko, C.P. Cabello, R. Ryoo, J. Čejka, Surfactant-directed mesoporous zeolites with enhanced catalytic activity in tetrahydropyranylation of alcohols: Effect of framework type and morphology, Applied Catalysis A: General, 537 (2017) 24-32.
[41] B. Wichterlová, Z. Tvarůžková, Z. Sobalík, P. Sarv, Determination and properties of acid sites in H-ferrierite: A comparison of ferrierite and MFI structures, Microporous and Mesoporous Materials, 24 (1998) 223-233.
[42] A. Zecchina, C.O. Arean, Diatomic molecular probes for mid-IR studies of zeolites, Chemical Society Reviews, 25 (1996) 187-197.
[43] L. Dimitrov, M. Mihaylov, K. Hadjiivanov, V. Mavrodinova, Catalytic properties and acidity of ZSM-12 zeolite with different textures, Microporous and Mesoporous Materials, 143 (2011) 291-301.

[44] W. Zhang, E.C. Burckle, P.G. Smirniotis, Characterization of the acidity of ultrastable Y, mordenite, and ZSM-12 via NH3-stepwise temperature programmed desorption and Fourier transform infrared spectroscopy, Microporous and Mesoporous Materials, 33 (1999) 173-185.
[45] W. Wu, W. Wu, O.V. Kikhtyanin, L. Li, A.V. Toktarev, A.B. Ayupov, J.F. Khabibulin, G.V. Echevsky, J. Huang, Methylation of naphthalene on MTW-type zeolites. Influence of template origin and substitution of Al by Ga, Applied Catalysis A: General, 375 (2010) 279-288.